ACS APPLIED MATERIALS & INTERFACES

Research Article

www.acsami.org

Laterally Expanded Rylene Diimides with Uniform Branched Side Chains for Solution-Processed Air Stable n-Channel Thin Film Transistors

Chengyi Xiao,[†,‡] Wei Jiang,*[,†] Xiangguang Li,[†,‡] Linxiao Hao,[†] Chunming Liu,[†,‡] and Zhaohui Wang[†]

[†]Beijing National Laboratory for Molecular Sciences, Key Laboratory of Organic Solids, Institute of Chemistry, Chinese Academy of Sciences, Beijing 100190, China

[‡]University of Chinese Academy of Sciences, Beijing 100049, China

Supporting Information

ABSTRACT: Molecular packing motifs in solid states is the dominant factor affecting the n-channel organic field-effect transistors (OFETs). However, few systematic researches were performed in the different extensions of π-conjugated molecules with the uniform substitution effecting the molecular packing motifs. In this manuscript, OFET devices based on three latterally expanded rylene diimides end-functionalized with uniform 3-hexylundecyl substitution on the imide positions were systematically studied on the relationship of molecular stacking, film microstructure, and charge transport. As the π-conjugated systems expanded from doubly linked perylene diimide dimer (d-4CldiPDI, **1**), triply linked perylene diimide dimer (t-4CldiPDI, **2**), to hybrid array (NDI-PDI-NDI, **3**), their corresponding molecular packing motifs exhibited a divide: the optimized molecular configuration became more planar and *d* (001) spacing distances became larger, which resulted in a larger $\pi-\pi$ overlapping. Thus, an enhanced electron mobility was obtained. A typical n-channel field-effect characteristic was observed in thin film devices based on these molecules under ambient conditions. Especially, the hybrid system (**3**) with more planar and π-expanded aromatic backbone exhibited superior electron mobility approaching 0.44 $cm^2 V^{-1} s^{-1}$ and on/off ratio of 10^6 after optimal annealing in this study.

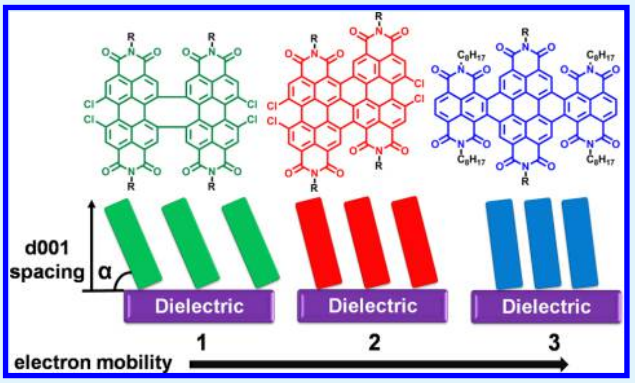

KEYWORDS: *lateral expansion, rylene diimides, uniform branched side chains, n-channel OFETs, molecular packing motifs, d-spacings*

INTRODUCTION

Organic field-effect transistors (OFETs) are of considerable interest for their advantages of lightweight, low-cost, and flexible processability as a potential replacement of silicon-based transistors or circuits.[1−4] OFET active materials can be divided into two classes according to the charges they transport (i.e., p-channel (holes) and n-channel (electrons)).[5] However, compared to p-channel counterparts, n-channel semiconductors have been far less developed.[6,7] High-performance, air-stable, and solution-processable n-channel organic semiconductors are a vital part for the real application of OFETs. It is well-known that charge mobility of n-channel semiconductors in OFETs is low because of many factors, including molecular packing, charge injection, environmental stability, etc.[8−10] Among these factors, molecular packing motifs in solid states is the chief factor effecting the overall device performances.[11−13] Organic semiconducting materials are generally composed of π-conjugated cores and attached side chains; thus, two strategies around the two parts are expected to improve the molecular packing motifs of n-channel semiconductors. Nevertheless, most efforts have been focused on the design of a new building block decorated with various side chains.[14−16] There is little systematic research on the different extensions of π-conjugated aromatic skeletons with the same substituent.[17]

Rylene dyes, especially naphthalene diimide (NDI) and perylene diimide (PDI) derivatives,[18−24] are being well developed as promising n-type organic semiconductors owing to their excellent photo- and thermal-stability, high electron affinities, and ease of chemical modification.[25−27] Lateral expansion of the rylene framework with different bay-linkages is deeply investigated in our group.[17,28−30] Expansion along the lateral positions will lead to the different degrees of twisting in the backbones due to the steric congestion between the fused rylene units; thereby, molecular packing motifs in solid states are significantly affected by that. Especially, doubly- or triply linked PDI oligomers, or hybrid NDI-PDI-NDI oligomers, showed remarkably different superstructures and $\pi-\pi$ stacking space, which led to a huge divide in charge mobility.

Received: July 28, 2014
Accepted: September 24, 2014
Published: September 24, 2014

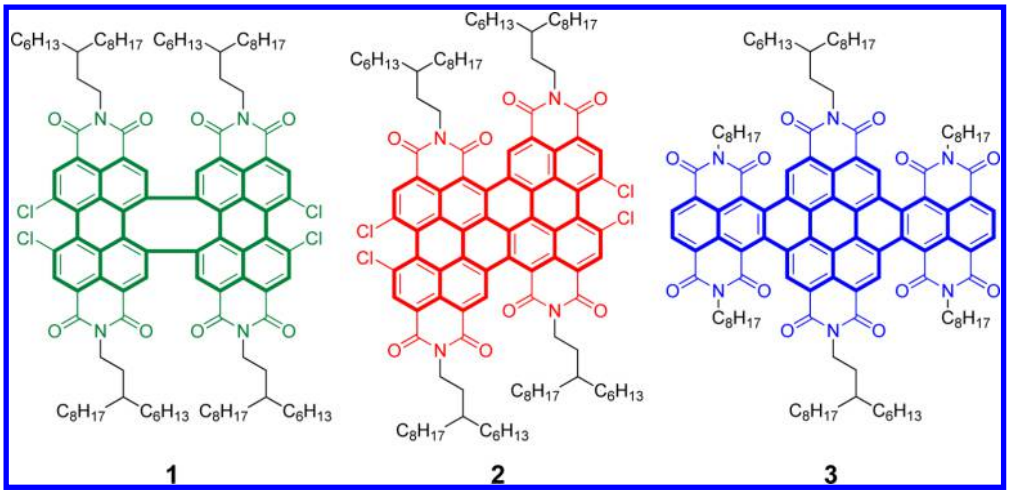

Figure 1. Chemical structures of laterally expanded rylene diimides in this study.

Table 1. Optical, Electrochemical, and Thermal Properties of Laterally Expanded Rylene Diimides 1−3

compd.	λ_{max}^{sol} (nm)[a]	ε (M^{-1} cm^{-1})[a]	λ_{max}^{film} (nm)[b]	E_{1r} (V)[c]	E_{2r} (V)[c]	E_{3r} (V)[c]	E_{4r} (V)[c]	E_{onset} (V)[c]	E_{LUMO} (eV)[d]	E_g (eV)[e]	T_{deg} (°C)[f]
1	524	62654	530	−0.88	−1.00	−1.12	−1.23	−0.78	−4.02	2.25	412
2	654	61528	668	−0.59	−0.79	−1.48	−1.61	−0.52	−4.28	1.84	375
3	614	19265	671	−0.67	−0.80	−1.09	−1.25	−0.60	−4.20	1.90	430

[a]Measured in dilute $CHCl_3$ solution (1.0×10^{-5} M). [b]Measured in the films on quartz substrates (as-spun). [c]Half-wave potentials in CH_2Cl_2 solution vs Fc/Fc^+, performed in n-Bu_4NPF_6/CH_2Cl_2 (0.1 M), scan rate 100 mV/s. [d]LUMO estimated by the onset of reduction peaks and calculated according to $E_{LUMO} = -(4.8 + E_{onset})$. [e]Calculated by the onset of absorption in $CHCl_3$ solution according to $E_g = 1240/\lambda_{onset}$. [f]Decomposition temperature determined by TGA corresponding to 5% weight loss at 10 °C min^{-1} under nitrogen flow.

Furthermore, lateral expansion in rylenes will lower the LUMO energy levels to a better electron injection and a material insensitive to water and oxygen.[31]

In this work, a family of laterally expanded rylene dyes based on different degrees of conjugated skeletons with the same 3-hexylundecyl substituents on their imide positions was designed, synthesized, characterized, and their corresponding thin film transistors (TFTs) were presented (Figure 1). As the π-conjugated molecular cores became larger, it was difficult to achieve a high-crystalline thin film. However, illustrated by the out-of-plane X-ray diffraction (XRD), their corresponding d (001) spacing distance became bigger, which led to a larger $\pi-\pi$ overlapping and an enhanced mobility. The larger d (001) spacing may attribute to a more planar molecular configuration shown by the previous theoretical calculations. Correspondingly, a TFT incorporating hybrid NDI-PDI-NDI (**3**) exhibited excellent electron mobility of 0.44 cm^2 V^{-1} s^{-1}, an on/off ratio of 10^6 when annealing at 220 °C. Larger aromatic systems are confirmed to be a remarkable strategy to tune the molecular packing motifs of organic semiconductors and their corresponding electronic properties.

EXPERIMENTAL SECTION

Synthetic routes illustrated in Supporting Information Scheme S1 of d-4CldiPDI (**1**)[17,29,32] and t-4CldiPDI (**2**),[28,31,33] which were synthesized by one-step of homocoupling of 4ClPDI (**4**) in moderate yields through Ullmann coupling (C−H transformation). While NDI-PDI-NDI (**3**)[30] was synthesized by one-step of cross-coupling reacting with 2-stannyl NDI via Stille coupling. All of the compounds are solids and could be easily purified by silica gel column chromatography and further unambiguously characterized by mass spectrometry (MS) and NMR spectroscopy. They are quite soluble in common solvents, such as dichloromethane, chloroform, tetrahydrofuran, toluene, and chlorobenzene, which means that they are feasible for solution-processed thin-film transistors.

All chemicals were purchased from commercial suppliers and used without further purification unless otherwise specified. The solvent DMSO from Alfa Aesar was dry and used directly, and toluene was distilled over sodium and benzophenone. ^1H NMR (400 MHz) and ^{13}C NMR (100 MHz) spectra were recorded in deuterated solvents on a Bruker ADVANCE 400 NMR Spectrometer. J values are expressed in Hz and quoted chemical shifts are in ppm downfield from tetramethylsilane (TMS) reference using the residual protonated solvent as an internal standard. Mass spectra (MALDI-TOF-MS) were determined utilizing a Bruker BIFLEX III mass spectrometer. Absorption spectra were measured with a Hitachi (model U-3010) UV−vis spectrophotometer in a 1 cm quartz cell. Cyclic voltammograms (CVs) were recorded using a Zahner IM6e electrochemical workstation at a scan rate of 100 mV s^{-1}, using glassy carbon discs as the working electrodes, Pt wire as the counter electrode, Ag/AgCl electrode as the reference electrode. Tetrabutylammoniumhexafluorophosphate (Bu_4NPF_6) (0.1 M) dissolved in CH_2Cl_2 (HPLC grade) was employed as the supporting electrolyte, which was calibrated by the ferrocene/ferrocenium (Fc/Fc^+) as the redox couple. CH_2Cl_2 was freshly distilled prior to use. Thermogravimetric analysis (TGA) measurements were performed on a PE TGA-7 instrument under a dry nitrogen flow, heating from room temperature to 550 °C, at a heating rate of 10 °C/min and the reported decomposition temperatures represent the temperatures observed at 5% mass loss. Differential scanning calorimetry (DSC) analyses were performed on a Mettler differential scanning calorimeter (DSC822E) under a dry nitrogen flow, heating from 0 to 350 °C and cooling from 350 to 0 °C at a rate of 10 °C/min. Atomic force microscopy (AFM) measurements were carried out with a Nanoscope IIIa instrument (Digital Instruments). X-ray diffraction (XRD) was measured on a D/max2500 with a Cu Kα source (κ = 1.541 Å).

The OFET characteristics were measured in air at room temperature using a Keithley 4200 SCS semiconductor parameter analyzer. The mobilities were calculated from the saturation region with the following equation: $I_{DS} = (W/2L)C_i\mu(V_G-V_T)^2$, where I_{SD} is

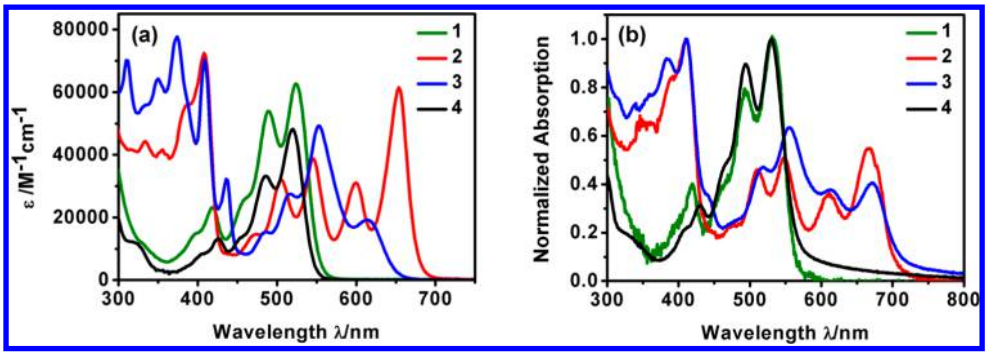

Figure 2. (a) UV−vis absorption spectra of compounds **1**−**4** in $CHCl_3$ solution (1×10^{-5} mol/L). (b) UV−vis absorption spectra in film of compounds **1**−**4**.

the drain−source current, W is the channel width, L is the channel length, μ is the field-effect mobility, C_i is the capacitance per unit area of the gate dielectric layer, and V_G and V_T are the gate voltage and threshold voltage, respectively. This equation defines the important characteristics of electron mobility (μ), on/off ratio ($I_{on/off}$), and threshold voltage (V_T), which could be deduced by the equation from the plot of current−voltage. For device fabrication, a layer of single-molecular semiconductor film (about 40 nm) was deposited on the octadecyltrichlorosilane (OTS) modified SiO_2/Si substrates.

RESULTS AND DISCUSSION

Optical, Electrochemical, and Thermal Properties. Table 1 summarizes the optical, electrochemical, and thermal properties of the laterally expanded rylene diimides. The thermal properties of these laterally expanded rylene diimides were investigated by TGA and DSC measurements under nitrogen atmosphere. Illustrated by the TGA and DSC analysis (see Supporting Information Figures S1 and S2), all of the compounds are thermally and oxidatively stable above 370 °C. Figure 2(a and b) shows UV−vis absorption spectra of compounds **1**−**4** in chloroform solution and in thin films at room temperature. Impressively, there were considerable broad and complicated absorption in molecules **1**−**3** relative to monomer **4**, probably as a reflection of different degrees of conjugation over the π-electronic systems with fine-tuned flexible annulation.[17] The spectra of compounds **1**−**3** appending same imide substituents showed the completely different major bands of about 524 nm, 654 nm, and 614 nm, which would bathochromically shifted to 530 nm, 668 nm, and 671 nm in films, suggesting that a certain degree of aggregation is present in films. Furthermore, the red shifts of low energy transition varied enormously from 6 to 14 and 57 nm in these films as the π-conjugated system extended from d-diPDI (**1**) to t-diPDI (**2**) and NDI-PDI-NDI (**3**), indicating a stronger $\pi-\pi$ stacking interaction.

The electrochemical properties of these laterally expanded rylene dyes were investigated by cyclic voltammograms (CVs) in dichloromethane (vs Fc/Fc^+). Seen in Supporting Information Figure S3, four well-defined single-electron reversible reduction waves were observed in the solvent/electrolyte window for compounds **1**−**3**. Their LUMO levels are below −4.0 eV, promising for ambient-stable electron transport n-channel OTFT semiconductors.[34−36] Moreover, the LUMO levels were lowered in turn as the π-conjugated systems became larger.

OFET Characterization. To investigate the thin film field-effect properties of this series of materials, a bottom-gate top-contact device configuration was afforded. Films of the semiconductors were spin-coated from $CHCl_3$ solution (10 mg/mL, 3000 r/min, 40−60 nm) onto Si/SiO_2 (300 nm) substrates modified with octadecyltrichlorosilane (OTS). Source/drain electrodes with width/length of 240 μm/30 μm were deposited on the semiconductor films through a shadow mask. All devices were measured under ambient conditions. Table 2 summarizes the FET characteristics of the devices

Table 2. Device Performance of Thin-Film Transistors for Compounds 1−3 at Optimized Annealing Temperature in Air

compd.	T (°C)[a]	μ_e (cm^2 V^{-1} s^{-1})[b]	V_T (V)[c]	I_{on}/I_{off}[d]
1	220	0.05	68.9	1.0×10^5
2	180	0.08	29.4	4.0×10^6
3	220	0.44	49.0	3.0×10^6

[a]Optimized annealing temperature. [b]Electron mobility. [c]Threshold voltage. [d]On/off current ratio.

evaluated under ambient conditions without any precautions to eliminate air and moisture at their optimized annealing temperature.

All of the compounds perform as n-type semiconductors. Figure 3 shows the representative transfer characteristics (I_{DS} versus V_{GS} plotted on a logarithmic scale and $(I_{DS})^{1/2}$ versus V_{GS}, at V_{DS} = 100 V) and output characteristics (I_{DS} vs V_{DS} at several values of V_{GS}) of the transistor devices based on compounds **2** and **3** at their optimized annealling temperatures. The electron mobilities of these laterally rylene diimides with uniform 3-hexylundecyl alkyl chain in the saturation regime were sensitive to the annealing temperature. For example, an exciting device performance of compound **3** with a maximum electron mobility of 0.44 cm^2 V^{-1} s^{-1} was achieved when annealing at 220 °C. However, this value slightly decreased to 0.23 cm^2 V^{-1} s^{-1} when raising the temperature up to 240 °C, which was accordance with the AFM image. Crystalline boundary density could trap a large number of charge carriers, which might have a significant effect on charge carrier mobility in OFET devices. As shown in Figure 4, it was found to have bigger crystalline boundaries and even cracks after annealing at 240 °C.

We also found an increased maximum electron mobilities from 0.05 cm^2 V^{-1} s^{-1}, 0.08 cm^2 V^{-1} s^{-1}, and 0.44 cm^2 V^{-1} s^{-1} as the core structure expanded from d-4CldiPDI (**1**) to t-4CldiPDI (**2**) and NDI-PDI-NDI (**3**). It is obvious that the larger π-conjugated semiconductor showed a higher electron mobility. In the case of compounds **2** and **3**, the electron mobility increased nearly 1 order of magnitude, and an exciting device performance with a maximum electron mobility of 0.44

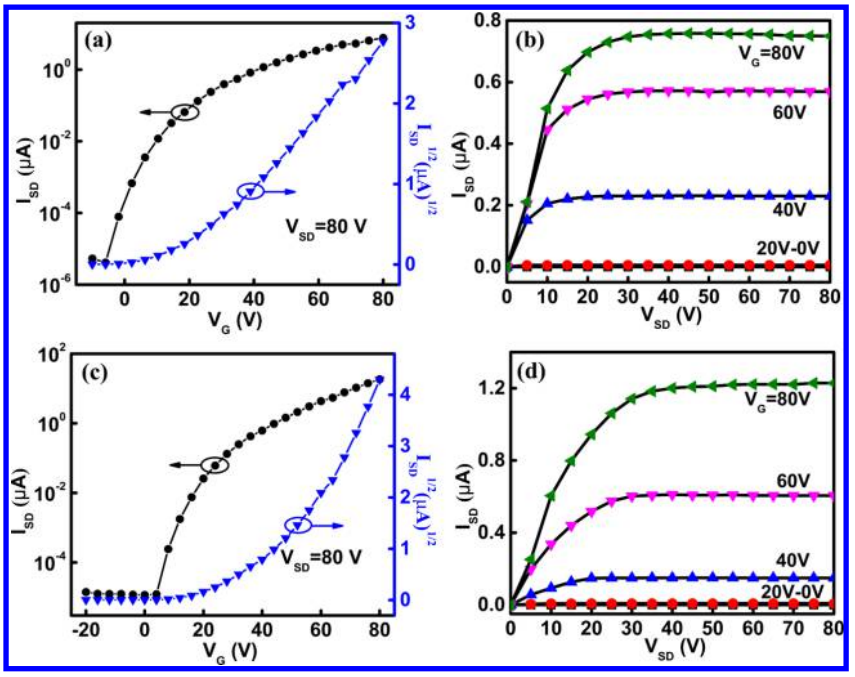

Figure 3. Representative transfer and output characteristics for OTFT devices based on compound **2** (a, b), and **3** (c, d) measured under ambient conditions.

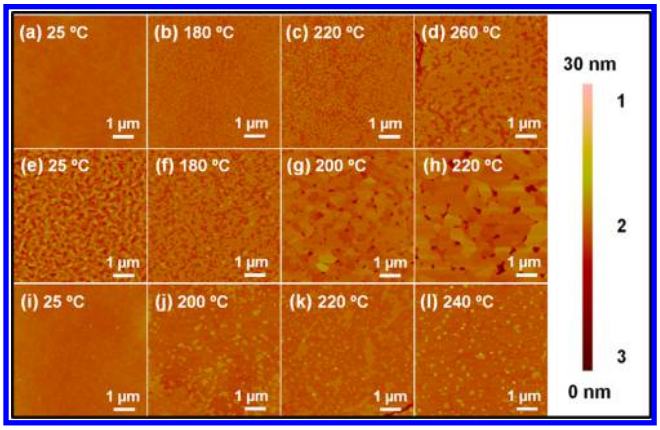

Figure 4. Comparison of AFM images of thin films of d-4CldiPDI (**1**, a–d), t-4CldiPDI (**2**, e–h), and NDI-PDI-NDI (**3**, i–l) at different annealing temperatures.

cm^2 V^{-1} s^{-1} with an on/off current ratio up to 3.5 × 10^6 was achieved for compound **3** after annealing at 220 °C.

Thin Film Morphology. The device performance is intensely affected by the film morphology. To investigate the thin film microstructures, molecular stacking motifs and correlating FET performance of these three molecules, X-ray diffraction (XRD) and atomic force microscopy (AFM) experiments were performed. As shown in Figure 4, thin films of NDI-PDI-NDI (**3**) exhibit a temperature-dependent morphology: crystalline grains become bigger and grain boundaries get larger as the temperature elevated, agreeing with the variation of mobilities. This phenomenon can also be reflected in XRD as shown in Supporting Information Figure S6, which shows more and more intense *d* spacing peak in pace with the increased temperature. Compounds **1** and **2** exhibit the similar temperature-dependent morphology. However, AFM images of t-4CldiPDI (**2**) exhibit bigger crystalline grains and better crystallinity than that of d-4CldiPDI (**1**) and NDI-PDI-NDI (**3**), accordance with the XRD measurement. An out-of-order films of compound **1** may attribute to its perpendicularly entangled molecular configuration. Nevertheless, the largest extension core in compound **3** would lead to the disorder in films.

We assumed the family of diffraction peaks to be *00l* according to other *n*-alkyl PDIs on the basis of single-crystal diffraction data of PDIs,[10] as we did not get the crystal structure of these compounds. According to Figure 5, thin films of

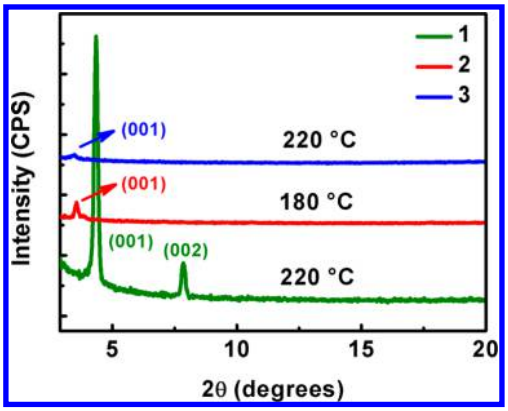

Figure 5. Comparison of XRD images of thin films of **1**–**3** at their best performance annealing temperature.

compounds **1**–**3** show an interlayer diffraction peak at 2θ = 3.72°, 3.56°, 3.48°, with a *d* (001) spacing distance of 24.1 Å, 24.8 Å, 25.4 Å, respectively, which accordance well with the length of PDIs, showing the edge-on orientation and a highly ordered layer-by-layer lamellar packing motif. Illustrated in Table 3, which summarized the *d* (001) spacing angles and distances of compounds **1**–**3**, as the π-conjugated systems extended from doubly linked diPDI to triply linked diPDI and hybrid NDI-PDI-NDI, their corresponding *d* spacing distance became bigger. Considering that compounds **1**–**3** have the

dx.doi.org/10.1021/am504984z | ACS Appl. Mater. Interfaces 2014, 6, 18098–18103

Table 3. *d* Spacing Distance for Compounds 1−3 Determined by XRD Data at Optimized Annealing Temperature in Air

compd.	T (°C)[a]	d (Å)[b]	2θ (deg)[c]
1	220	24.1	3.72
2	180	24.8	3.56
3	220	25.4	3.48

[a]Optimized annealing temperature. [b]The *d* spacing angles. [c]The *d* spacing distances.

uniform branched side chains, molecular length of them are almost the same. As the *d* spacing distances became larger (shown in Figure 6) and *d* (001) spacing angle between

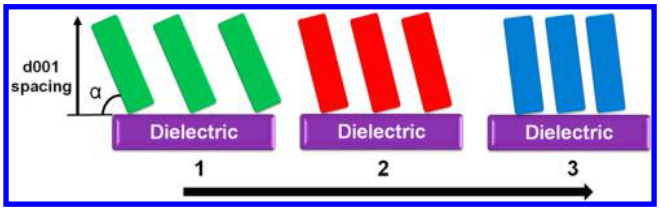

Figure 6. Schematic diagram of molecular packing motifs of compounds **1**−**3** at their optimized annealing temperatures.

molecular and the substrate became larger, a more tightly molecular stacking was available, which further gave rise to a larger $\pi-\pi$ overlapping and an enhanced electron mobility.[37,38]

The B3LYP-optimized geometries of compounds **1**−**3** had been investigated in our previous work.[28−30,32,33] The optimized molecular configuration of doubly linked diPDI **1** was found to be almost perpendicular, which would lead to a smaller π orbital overlap and result in a lower electron mobility in OFET devices. The most planar optimized geometry of molecule **3** explained the impressive high electron mobility of 0.44 $cm^2\ V^{-1}\ s^{-1}$. Larger aromatic systems were confirmed to be more planar because of the delocalization of electronics and have a relatively bigger *d* (001) spacing distance and larger π orbital overlap, and eventually gave rise to a higher mobility.

CONCLUSION

A new family of laterally expanded rylene diimides with different skeletons featuring uniform branching alkyl substitution on the imide positions were designed and synthesized. All of the compounds are suitable for solution processes, implying their superior solubility in organic solvents. Thermal, optical, and electrochemical properties are measured by UV−vis absorption spectra, TGA, DSC, and cyclic voltammetry measurements, respectively. To investigate the thin film field-effect properties of the series of materials, a bottom-gate top-contact device configuration was afforded. As the π-conjugated systems extended from doubly linked diPDI (d-4CldiPDI, **1**) to triply linked diPDI (t-4CldiPDI, **2**) and hybrid NDI-PDI-NDI (**3**), their corresponding *d* spacing distances became larger and molecular configuration shown by previous theoretical calculation seemed to be more planar, which resulted in a larger $\pi-\pi$ overlapping and an enhanced electron mobility. Especially, a TFT incorporating NDI-PDI-NDI (**3**) exhibited excellent field effect mobility of 0.44 $cm^2\ V^{-1}\ s^{-1}$, an on/off ratio of 10^6 after optimized annealing.

ASSOCIATED CONTENT

Supporting Information

Detailed synthetic procedures, TGA, DSC, CV, AFM, NMR, MS, and representative transfer curves of other compounds. This material is available free of charge via the Internet at http://pubs.acs.org.

AUTHOR INFORMATION

Corresponding Author

*Email: jiangwei@iccas.ac.cn.

Notes

The authors declare no competing financial interest.

ACKNOWLEDGMENTS

For financial support of this research, we thank the National Natural Science Foundation of China (21225209, 91027043, and 21190032), 973 Program (Grants 2011CB932301, 2012CB932903, and 2013CB933503), NSFC-DFG Joint Project TRR61, and the Chinese Academy of Sciences (XDB12010400).

REFERENCES

(1) Wang, C.; Dong, H.; Hu, W.; Liu, Y.; Zhu, D. Semiconducting π-Conjugated Systems in Field-Effect Transistors: A Material Odyssey of Organic Electronics. *Chem. Rev.* **2011**, *112*, 2208−2267.

(2) Jiang, W.; Li, Y.; Wang, Z. Heteroarenes as High Performance Organic Semiconductors. *Chem. Soc. Rev.* **2013**, *42*, 6113−6127.

(3) Zhan, X.; Facchetti, A.; Barlow, S.; Marks, T. J.; Ratner, M. A.; Wasielewski, M. R.; Marder, S. R. Rylene and Related Diimides for Organic Electronics. *Adv. Mater.* **2011**, *23*, 268−284.

(4) Tucker, N. M.; Briseno, A. L.; Acton, O.; Yip, H.-L.; Ma, H.; Jenekhe, S. A.; Xia, Y.; Jen, A. K.-Y. Solvent-Dispersed Benzothiadiazole-Tetrathiafulvalene Single-Crystal Nanowires and Their Application in Field-Effect Transistors. *ACS Appl. Mater. Interfaces* **2013**, *5*, 2320−2324.

(5) Klauk, H. Organic Thin-Film Transistors. *Chem. Soc. Rev.* **2010**, *39*, 2643−2666.

(6) Li, H.; Tee, B. C.; Giri, G.; Chung, J. W.; Lee, S. Y.; Bao, Z. High-Performance Transistors and Complementary Inverters Based on Solution-Grown Aligned Organic Single-Crystals. *Adv. Mater.* **2012**, *24*, 2588−2591.

(7) Zhao, Y.; Guo, Y.; Liu, Y. 25th Anniversary Article: Recent Advances in n-Type and Ambipolar Organic Field-Effect Transistors. *Adv. Mater.* **2013**, *25*, 5372−5391.

(8) Naab, B. D.; Himmelberger, S.; Diao, Y.; Vandewal, K.; Wei, P.; Lussem, B.; Salleo, A.; Bao, Z. High Mobility n-Type Transistors Based on Solution-Sheared Doped 6,13-Bis(triisopropylsilylethynyl)-pentacene Thin Films. *Adv. Mater.* **2013**, *25*, 4663−4667.

(9) Dong, H.; Wang, C.; Hu, W. High Performance Organic Semiconductors for Field-Effect Transistors. *Chem. Commun.* **2010**, *46*, 5211−5222.

(10) Jones, B. A.; Facchetti, A.; Wasielewski, M. R.; Marks, T. J. Tuning Orbital Energetics in Arylene Diimide Semiconductors. Materials Design for Ambient Stability of n-Type Charge Transport. *J. Am. Chem. Soc.* **2007**, *129*, 15259−15278.

(11) He, T.; Stolte, M.; Würthner, F. Air-Stable n-Channel Organic Single Crystal Field-Effect Transistors Based on Microribbons of Core-chlorinated Naphthalene Diimide. *Adv. Mater.* **2013**, *25*, 6951−6955.

(12) Zhao, G.; Dong, H.; Zhao, H.; Jiang, L.; Zhang, X.; Tan, J.; Meng, Q.; Hu, W. Substitution Effect on Molecular Packing and Transistor Performance of Indolo[3,2-*b*]carbazole Derivatives. *J. Mater. Chem.* **2012**, *22*, 4409−4417.

(13) Chen, H.; Guo, Y.; Yu, G.; Zhao, Y.; Zhang, J.; Gao, D.; Liu, H.; Liu, Y. Highly π-Extended Copolymers with Diketopyrrolopyrrole

Moieties for High-Performance Field-Effect Transistors. *Adv. Mater.* **2012**, *24*, 4618−4622.
(14) Lei, T.; Dou, J. H.; Pei, J. Influence of Alkyl Chain Branching Positions on the Hole Mobilities of Polymer Thin-Film Transistors. *Adv. Mater.* **2012**, *24*, 6457−6461.
(15) Zhang, F.; Hu, Y.; Schuettfort, T.; Di, C. A.; Gao, X.; McNeill, C. R.; Thomsen, L.; Mannsfeld, S. C.; Yuan, W.; Sirringhaus, H.; Zhu, D. Critical Role of Alkyl Chain Branching of Organic Semiconductors in Enabling Solution-Processed n-Channel Organic Thin-Film Transistors with Mobility of up to 3.50 $cm^2 V^{-1} s^{-1}$. *J. Am. Chem. Soc.* **2013**, *135*, 2338−2349.
(16) Zhang, J.; Ma, Z.; Zhang, Q.; Virk, T. S.; Geng, H.; Wang, D.; Xu, W.; Shuai, Z.; Singh, K.; Hu, W.; Zhu, D. Substitution Effects on the Electrical Tranporting Properties of Tetrathia[22]annulene-[2,1,2,1]: Experimental and Theoretical Investigations. *J. Mater. Chem. C* **2013**, *1*, 5765−5771.
(17) Jiang, W.; Xiao, C.; Hao, L.; Wang, Z.; Ceymann, H.; Lambert, C.; Di Motta, S.; Negri, F. Localization/Delocalization of Charges in Bay-Linked Perylene Bisimides. *Chem.—Eur. J.* **2012**, *18*, 6764−6775.
(18) Jung, B. J.; Martinez Hardigree, J. F.; Dhar, B. M.; Dawidczyk, T. J.; Sun, J.; See, K. C.; Katz, H. E. Naphthalenetetracarboxylic Diimide Layer-Based Transistors with Nanometer Oxide and Side Chain Dielectrics Operating below 1 V. *ACS Nano* **2011**, *5*, 2723−2734.
(19) Figueira-Duarte, T. M.; Müllen, K. Pyrene-Based Materials for Organic Electronics. *Chem. Rev.* **2011**, *111*, 7260−7314.
(20) Yan, H.; Chen, Z.; Zheng, Y.; Newman, C.; Quinn, J. R.; Dötz, F.; Kastler, M.; Facchetti, A. A High-Mobility Electron-Transporting Polymer for Printed Transistors. *Nature* **2009**, *457*, 679−686.
(21) Li, C.; Xiao, C.; Li, Y.; Wang, Z. Synthesis and Properties of Heterocyclic Acene Diimides. *Org. Lett.* **2013**, *15*, 682−685.
(22) Guo, X.; Kim, F. S.; Seger, M. J.; Jenekhe, S. A.; Watson, M. D. Naphthalene Diimide-Based Polymer Semiconductors: Synthesis, Structure-Property Correlations, and n-Channel and Ambipolar Field-Effect Transistors. *Chem. Mater.* **2012**, *24*, 1434−1442.
(23) Chen, S. C.; Ganeshan, D.; Cai, D.; Zheng, Q.; Yin, Z.; Wang, F. High Performance n-Channel Thin-Film Field-Effect Transistors Based on Angular-Shaped Naphthalene Tetracarboxylic Diimides. *Org. Electron.* **2013**, *14*, 2859−2865.
(24) Kim, R.; Amegadze, P. S. K.; Kang, I.; Yun, H.-J.; Noh, Y.-Y.; Kwon, S.-K.; Kim, Y.-H. High-Mobility Air-Stable Naphthalene Diimide-Based Copolymer Containing Extended π-Conjugation for n-Channel Organic Field Effect Transistors. *Adv. Funct. Mater.* **2013**, *23*, 5719−5727.
(25) Jung, B. J.; Tremblay, N. J.; Yeh, M.-L.; Katz, H. E. Molecular Design and Synthetic Approaches to Electron-Transporting Organic Transistor Semiconductors. *Chem. Mater.* **2010**, *23*, 568−582.
(26) Katz, H. E.; Lovinger, A. J.; Johnson, J.; Kloc, C.; Siegrist, T.; Li, W.; Lin, Y. Y.; Dodabalapur, A. A Soluble and Air-Stable Organic Semiconductor with High Electron mobility. *Nature* **2000**, *404*, 478−481.
(27) Suraru, S. L.; Würthner, F. Regioselectivity in Sequential Nucleophilic Substitution of Tetrabromonaphthalene Diimides. *J. Org. Chem.* **2013**, *78*, 5227−5238.
(28) Qian, H.; Wang, Z.; Yue, W.; Zhu, D. Exceptional Coupling of Tetrachloroperylene Bisimide: Combination of Ullmann Reaction and C−H Transformation. *J. Am. Chem. Soc.* **2007**, *129*, 10664−10665.
(29) Zhen, Y.; Yue, W.; Li, Y.; Jiang, W.; Di Motta, S.; Di Donato, E.; Negri, F.; Ye, S.; Wang, Z. Chiral Nanoribbons Based on Doubly-Linked Oligo-Perylene Bisimides. *Chem. Commun.* **2010**, *46*, 6078−6080.
(30) Yue, W.; Lv, A.; Gao, J.; Jiang, W.; Hao, L.; Li, C.; Li, Y.; Polander, L. E.; Barlow, S.; Hu, W.; Di Motta, S.; Negri, F.; Marder, S. R.; Wang, Z. Hybrid Rylene Arrays via Combination of Stille Coupling and C−H Transformation as High-Performance Electron Transport Materials. *J. Am. Chem. Soc.* **2012**, *134*, 5770−5773.
(31) Zhang, J.; Tan, L.; Jiang, W.; Hu, W.; Wang, Z. N-Alkyl Substituted Di(perylene bisimides) as Air-Stable Electron Transport Materials for Solution-Processible Thin-Film Transistors with Enhanced Performance. *J. Mater. Chem. C* **2013**, *1*, 3200−3206.
(32) Hao, L.; Xiao, C.; Zhang, J.; Jiang, W.; Xu, W.; Wang, Z. Perpendicularly Entangled Perylene Diimides for High Performance Electron Transport Materials. *J. Mater. Chem. C* **2013**, *1*, 7812−7818.
(33) Lv, A.; Puniredd, S. R.; Zhang, J.; Li, Z.; Zhu, H.; Jiang, W.; Dong, H.; He, Y.; Jiang, L.; Li, Y.; Pisula, W.; Meng, Q.; Hu, W.; Wang, Z. High Mobility, Air Stable, Organic Single Crystal Transistors of an n-Type Diperylene Bisimide. *Adv. Mater.* **2012**, *24*, 2626−2630.
(34) Zöphel, L.; Enkelmann, V.; Müllen, K. Tuning the HOMO-LUMO Gap of Pyrene Effectively via Donor−Acceptor Substitution: Positions 4,5 Versus 9,10. *Org. Lett.* **2013**, *15*, 804−807.
(35) Polander, L. E.; Tiwari, S. P.; Pandey, L.; Seifried, B. M.; Zhang, Q.; Barlow, S.; Risko, C.; Brédas, J.-L.; Kippelen, B.; Marder, S. R. Stannyl Derivatives of Naphthalene Diimides and Their Use in Oligomer Synthesis. *Chem. Mater.* **2011**, *23*, 3408−3410.
(36) Wang, H.; Wen, Y.; Yang, X.; Wang, Y.; Zhou, W.; Zhang, S.; Zhan, X.; Liu, Y.; Shuai, Z.; Zhu, D. Fused-Ring Pyrazine Derivatives for n-Type Field-Effect Transistors. *ACS Appl. Mater. Interfaces* **2009**, *1*, 1122−1129.
(37) Giri, G.; Verploegen, E.; Mannsfeld, S. C.; Atahan-Evrenk, S.; Kim do, H.; Lee, S. Y.; Becerril, H. A.; Aspuru-Guzik, A.; Toney, M. F.; Bao, Z. Tuning Charge Transport in Solution-Sheared Organic Semiconductors Using Lattice Strain. *Nature* **2011**, *480*, 504−508.
(38) Rose, B. D.; Santa Maria, P. J.; Fix, A. G.; Vonnegut, C. L.; Zakharov, L. N.; Parkin, S. R.; Haley, M. M. Scalable Synthesis of 5,11-Diethynylated Indeno[1,2-*b*]fluorene-6,12-diones and Exploration of Their Solid State Packing. *Beilstein J. Org. Chem.* **2014**, *10*, 2122−2130.